J. exp. Biol. **155**, 585–603 (1991)
Printed in Great Britain © *The Company of Biologists Limited 1991*

FORCES GENERATED BY THE JAWS OF CLYPEASTEROIDS (ECHINODERMATA: ECHINOIDEA)

BY OLAF ELLERS*

Department of Zoology, Duke University, Durham, NC 27706, USA

AND MALCOLM TELFORD

Department of Zoology, University of Toronto, Toronto, Ontario, Canada, M5S 1A1

Accepted 12 July 1990

Summary

Aristotle's lantern acts like a five-toothed 'vice grip.' Contraction of the interpyramidal muscles creates tangential stresses that are converted to radial forces along the teeth. Two mechanical models are proposed to explain this conversion. In the first, the lantern is regarded as a thick-walled cylinder resisting internal pressure; in the second, it is treated as a cluster of wedges. The two models differ primarily in the allowance of radial forces within the muscle in the cylinder and their exclusion in the wedge model. Maximum muscle stress required for a given force along the teeth depends on the ratio of external to internal lantern radii (r_o/r_i). Maximal force requires that r_o/r_i should be greater than 2, which is the case in *Clypeaster rosaceus* (L.). The models allow calculation of a dimensionless number, $\mathscr{F}$, which scales the force exerted by the teeth for changes in lantern size and the number of pyramids. Biting force was measured in *C. rosaceus* and used to calculate the muscle stress required by the mechanical models. For the thick-walled cylinder, maximum interpyramidal muscle stress was calculated to be $2.8\times10^6\,N\,m^{-2}$. For the wedge model it was $1.9\times10^5\,N\,m^{-2}$. The models were supported by comparison of predicted with observed biting forces in another clypeasteroid, *Encope michelini* L. Agassiz.

Introduction

Aristotle's lantern is the principal feeding structure in many echinoids. In clypeasteroids it is a non-protrusible crushing device used to pulverize food material. In the familiar, globose regular urchins it operates like a five-toothed mechanical grab. The lantern of regular urchins is composed of forty skeletal elements including the teeth (Hyman, 1955) and an elaborate musculature (Lanzavecchia *et al.* 1988). Smith (1984) and Candia Carnevali *et al.* (1988) have

* Present address: Department of Zoology, University of California, Davis, CA 95616, USA.

Key words: Clypeasteroida, Aristotle's lantern, force measurement, mechanical model.

described its operation. The skeletal elements include ten half pyramids sutured to form five inverted pyramids located around the esophagus, each of which supports a tooth. The distal ends of the teeth pass through the wall of the esophagus and converge in the center of the mouth region. Each half-pyramid has an epiphysis sutured to its upper end. Between the epiphyses of adjacent pyramids are flattened rotules. Overlying the rotules are radially arranged compasses consisting of inner and outer ossicles.

Between the pyramids there are short, transverse fibers of interpyramidal or comminator muscles. Lantern protractor muscles extend from the epiphyses to the perignathic girdle encircling the peristome. These muscles lower the lantern so that the teeth may extend beyond the peristomial membrane. Retractor muscles, passing from the tips of the pyramids to the perignathic girdle, withdraw the lantern after protrusion and open the jaw by pulling the teeth apart. The small rotular muscles, attaching each rotule to the associated epiphyses, serve to align the pyramids following unequal movements.

With the exception of the Holectypoida and Clypeasteroida, adult irregular urchins do not possess a lantern but vestiges of it appear in juvenile cassiduloids (Kier, 1974; Smith, 1984; Mooi, 1987) and a few spatangoids. The clypeasteroid lantern has presumably been derived from these juvenile vestiges (Kier, 1974; Mooi, 1987). It is quite unlike the regular urchin lantern in several respects: compasses are absent, rotules and epiphyses are small and the entire lantern is somewhat squat and flat. The clypeasteroid lantern is not protrusible and the retractor muscles serve the single function of jaw openers while the protractors are regarded as 'postural' muscles (Smith, 1984). Although flattened, the clypeasteroid lantern is relatively large and the comminator muscles, which draw the pyramids together, are large in cross-sectional area. The morphology of clypeasteroid teeth has been described by Märkel (1970).

Lantern movements in regular echinoids are directed primarily towards feeding (Lawrence, 1987) but may also contribute to respiration (Hyman, 1955) or circulation of perivisceral coelomic fluid (Jensen, 1985). The role of the lantern in clypeasteroids appears to be solely for feeding. Analyses of clypeasteroid feeding (Ellers and Telford, 1984; Telford *et al.* 1983, 1985, 1987; Telford and Mooi, 1986) have shown that particles are collected by podia, passed to the food grooves and thence to the mouth. As they are ingested they are partially broken up by the lantern teeth (Telford *et al.* 1985).

The only previous explanation of lantern mechanics (Candia Carnevali *et al.* 1988) deals with movements of the lantern of regular urchins, not the forces produced during biting. In the present paper, we measure the radial forces generated by the lantern of *Clypeaster rosaceus* and compare them with forces necessary to break sand grains and other food material. We propose two analytical, mechanical models which explain how this force is produced. In both models, tangential stress from contraction of the comminator muscles is balanced by forces aligned radially along the teeth. One model proposes that the lantern generates forces in a manner analogous to a thick-walled cylinder resisting an

internal pressure. The other considers the lantern as a series of five wedges pulled together by the comminator muscles. The models differ in assumptions about the transfer of forces between the muscles and pyramids, and about the material properties of the pyramids. The models allow prediction of biting forces in all sizes of clypeasteroid lanterns, and this provides the basis for a limited test of their validity.

Materials and methods

Collection of animals

Specimens of *Clypeaster rosaceus* and *Encope michelini*, collected at Long Key, Florida, were maintained in outdoor aquaria with running sea water and a natural substratum. Specimens of *Mellita isometra* Harold and Telford, *Leodia sexiesperforata* (Leske) and *Echinarachnius parma* (Lamarck) were obtained from Beaufort, North Carolina; Holetown, Barbados and St Andrews, New Brunswick, respectively.

Morphological measurements

Lantern diameters of *C. rosaceus* were measured as in Fig. 1. The external radius was taken to be half the external diameter. The internal radius was taken as half the average of the internal diameters on the oral and aboral surfaces. The area of the interpyramidal muscle attachment (Fig. 2) was measured by tracing its outline with a digitizer. For all other species we measured the internal diameter of the lantern (on the aboral surface only) and the area of the radial projection of the

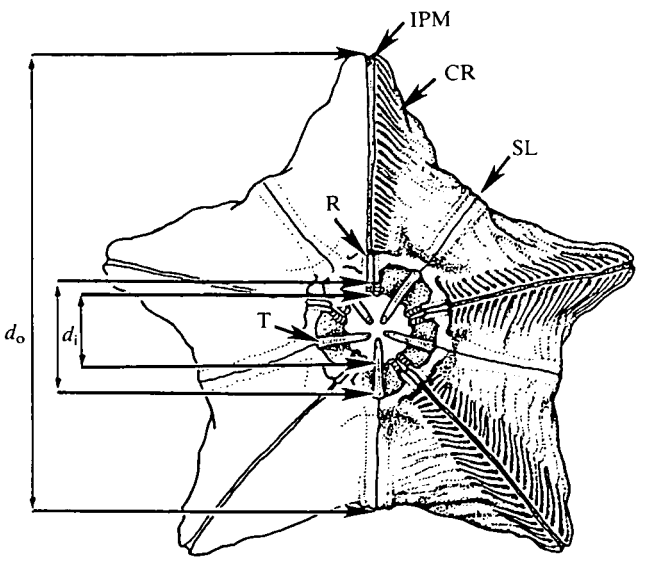

Fig. 1. Lantern of *Clypeaster rosaceus* (external diameter 52.7 mm), aboral view. IPM, interpyramidal muscle; CR, calcite ridges; SL suture line between half-pyramids; R, rotule; T, tooth; d_o, outside diameter; d_i, inside diameters measured orally and aborally (see text).

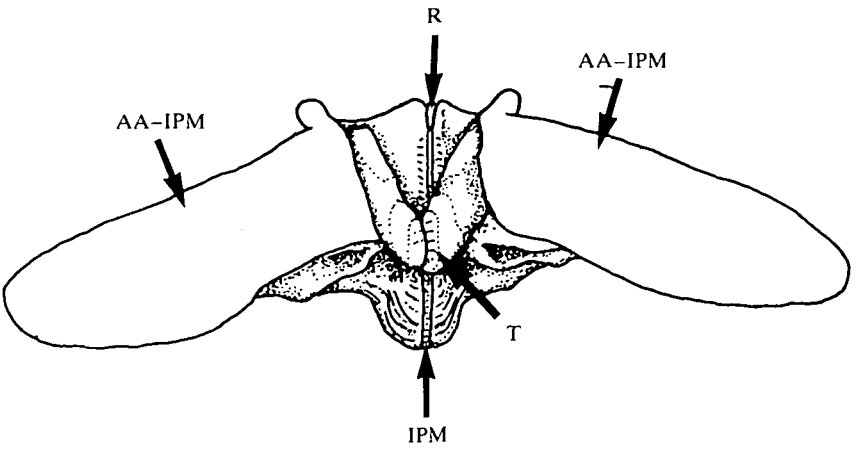

Fig. 2. Two adjacent pyramids and teeth (T) of *Clypeaster rosaceus* (external lantern diameter 52.7 mm), showing areas for attachment of interpyramidal muscles (AA–IPM), position of rotule (R) and interpyramidal muscle (IPM) between pyramids. Figs 3 and 4 show gradual abstractions to illustrate how this morphology is modelled.

plane where the tooth attaches to the pyramid. These morphological variables were used in subsequent calculations of muscle stress.

Mechanical tests

Biting capability of live Clypeaster rosaceus

Specimens were placed oral surface up under the stereomicroscope so that the teeth were visible when the peristomial membrane retracted. The following tests were performed.

(1) A length of solder was inserted into the mouth and the teeth allowed to close on it five times, at different locations. The duration of each bite was recorded. Tooth marks in the bitten solder were calibrated as described below.

(2) Several types of glass tube were inserted in the mouth: a coagulation tube (1.10 mm o.d.), and green (1.55 mm o.d.), white (1.25 mm o.d.) and double white (1.45 mm o.d.) colour-coded micropipets. On presentation, a tube was held in place and the teeth were allowed to close three times. If the tube was fractured, the next in the series was tried. If it was not broken, the tests were ended.

Calibration of bite forces

Teeth from *C. rosaceus* were removed by dissection, cut and glued to the platens of a materials tester assembled from component parts and referred to as a 'minicrusher'. The device was then used for calibration of all materials except the colour-coded pipets. For solder and other tests, the teeth of the minicrusher were brought together at 64 μm s^{-1}. The colour-coded pipets required forces greater than the range of the minicrusher (up to 50 N for these experiments) and were

therefore tested in an Instron model 1122 universal testing machine, using *C. rosaceus* teeth on platens driven together at 84 $\mu m\,s^{-1}$. These differences in rate of tooth closure had no observable effect on required breaking forces. The speeds were chosen to be of the same order of magnitude as tooth movements in living specimens.

Solder. Pieces of solder were indented at known forces ranging from 2.5 to 30.0 N. Under a stereomicroscope, the indentations were aligned transversely to an eyepiece reticule. A colour-banded Minuten insect pin was then aligned at 90° to the axis of the solder and propelled into the indentation by a micromanipulator. The distance travelled was recorded from the reticule and converted to micrometers. Each indentation was measured five times. A regression of depth (dependent variable) against force (independent variable), fitted by least squares using log-transformed data, was performed. The regression equation was used to calculate the force for each depth of bite produced by the experimental animals. Reading error in the measurement of depth was ±10 % for the smallest forces and ±2 % for the largest. Error in the force measurement was ±4 % for the smallest and ±0.5 % for the largest forces.

Glass tubes. The different types were calibrated by testing to destruction. The distribution of breaking strengths of each type was statistically tested and found to be normal, despite the small sample sizes (see Table 1). The force exerted by the animals was obtained by multiplying a *z*-score (determined from the fraction of tubes broken) (Sokal and Rohlf, 1981) by the standard deviation and adding it to the mean for each type of tube.

Food items. Substratum particles were tested in the same way. For ease of manipulation and identification, particles were chosen from the upper size range normally ingested by *C. rosaceus* (Telford *et al.* 1987). Ten pieces each of the coralline algae *Halimeda* and *Corallina* and mollusc shell fragments were measured by eye-piece micrometer. The pieces were fractured across the region of least thickness. In addition, ten spines of *Diadema antillarum* and ten of *Meoma ventricosa* were broken. For each type of material the mean, standard deviation, and minimum and maximum forces were obtained and compared with the forces measured along the teeth of *C. rosaceus*.

Biting behaviour of Encope michelini

Encope michelini has a smaller mouth opening than *C. rosaceus*, thus a different set of tests was necessary. Only three specimens were available. They were offered measured *Diadema* spines to bite, followed by glass microcells which were rectangular in cross-section. Forces to break the two sizes of microcell (0.10 mm×0.10 mm and 0.30 mm×0.15 mm) were determined in the minicrusher.

Siliceous sand particles

To estimate the forces that can be generated by the teeth of *M. isometra* we determined the forces required to break sediment particles from its habitat. Forty-four irregularly shaped, angular grains were measured and fractured between the

metal platens of the minicrusher. Force was applied through the smallest dimension (thickness). The course of the test was followed on a recording potentiometer and simultaneously by microscopic observation. Fractures of the particles were usually marked by sudden changes in refraction as well as interruptions of the chart record. Least-squares, linear bivariate and multivariate regressions of breaking force (dependent variable) and length, width and thickness (independent variable) were performed.

Results

Morphological measurements

Twelve specimens of *C. rosaceus* (111.3 mm×83.8 mm to 135.8 mm×116.2 mm) were used in the biting experiments. Complete lantern measurements were obtained from five. Outside diameters of the lanterns ranged from 50.1 to 58.5 mm, mean inside diameters from 11.7 to 14.2 mm. Cross-sectional areas of the anterior interpyramidal muscles ranged from 290 to 407 mm^2. The three specimens of *Encope michelini* measured 96.8 mm×95.2 mm, 101.7 mm×99.4 mm and 105.2 mm×104.1 mm. Outside diameters of the lanterns ranged from 19.7 to 22.9 mm, inside diameters from 3.98 to 4.50 mm. Cross-sectional areas of the interpyramidal muscles were not obtained from these specimens. However, interpyramidal muscle area of similar-sized animals was later determined and used in our wedge model to predict radial forces.

Determination of bite forces

Solder calibration

Regression of the calibration forces and solder indentations yielded the relationship: $\text{depth}=34.08\times10^{-6}\times\text{force}^{0.783}$, where depth is in meters and force is in newtons ($r^2=0.97$). Depths of indentations in experimental bite bars were measured five times each and the corresponding forces obtained from the above regression. The smallest biting force recorded for *C. rosaceus* was only 0.9 N, the greatest was 26.7 N and the mean, per animal, ranged from 2.8 to 14.9 N. Duration of the bites ranged from 10 to 158 s. There was no correlation between duration and force exerted.

Sources of error. Validity of the inference of force from depth of indentation depends on similarity of loading and the material properties of the solder. The occlusal surface of each tooth bears two unequal cusps, one above the other. Depending on the angle of tooth movement, either the lower or both cusps contacted the solder during a bite. In our minicrusher only the larger (lower cusp) penetrated the solder. Thus, the surface area of tooth in contact with the solder was usually lower in the calibration tests but greater than half of that in the bite experiments.

Area of contact is an important variable because solder deforms plastically at a constant stress over a large range of strains. Thus, as a tooth drives deeper into the solder the force increases not because the stress is increasing but because the area

over which the yield stress acts is increasing. It is not possible to survey this area accurately since it will be different each time depending on exactly how the stress is distributed through the material. The above regression calibrates this change in area as a function of depth. We used a variety of teeth at a variety of angles in our minicrusher and the unexplained variation in the regression includes differences due to loading and other factors. The 95% confidence intervals from the regression were used as an expression of lack of precision. This amounts to less than ±10% in the force implied from the depth of a bite mark. Because the contact area between the tooth and the solder was underestimated by at most a factor of two, a further factor of two can be added to the error as a bias, which is likely to underestimate the force the teeth can exert. The maximum force that *C. rosaceus* exerted on the solder was therefore between 24.0 N [26.7−(10%×26.7)] and 56.7 N [(26.7×2)+(10%×26.7)]. Error might also be introduced if the animals did not bite the solder as hard as they could. For another estimate of the maximum force that the teeth can exert we used glass tubes in place of solder.

Glass tubes

Data on the fracture of tubes during calibration tests and biting by *C. rosaceus* are in Table 1. These tests indicate that *C. rosaceus* can develop crushing forces that may exceed 100 N.

Forces to fracture food items

Forces required to fracture common food items are shown in Table 2. Some pieces of mollusc shell could not be broken by us because they required forces beyond the capacity of the strain gauge used (50 N). If *C. rosaceus* applies forces of the magnitude implied by solder bite bars, the animals would fracture most of the food particles commonly encountered, except for some fragments of mollusc shell (Table 2). Based on the forces inferred from fracturing glass tubes, it appears likely that *C. rosaceus* could pulverize even these fragments.

Fracture of siliceous sand grains

Of the forty-four sand grains tested, ranging from 273 μm×182 μm×127 μm to

Table 1. *Breaking strengths of glass tubes and inferred forces generated by lanterns of* Clypeaster rosaceus

Type of tube (sample size)	Mean breaking force±S.D. (N)	Fraction broken (sample size)	Inferred force (N)
Coagulation (13)	28.6±7.9	0.75 (12)	33
Green pipet (30)	167.0±66.0	0.28 (18)	40
White pipet (26)	114.0±57.0	0.50 (10)	114
Double white pipet (38)	75.5±19.0	0.57 (7)	79

Inferred lantern force was obtained from the fraction of tubes broken in the tests by *C. rosaceus* (see text for details).

Table 2. *Forces required to fracture common food items of the sea biscuit* Clypeaster rosaceus

Food items (N=10)	Minimum force (N)	Maximum force (N)	Mean force ±S.D. (N)
Meoma spines	0.8	1.9	1.4±0.3
Diadema spines	2.4	5.1	3.3±0.9
Halimeda flakes	0.6	9.8	3.9±2.7
Corallina pieces	0.2	24.2	8.6±9.0
Mollusc shell	4.8	>50	19.0±8.8

819 μm×546 μm×455 μm, two did not break, implying a required force larger than 15 N (test-limit of the strain gauges used). The maximum force that broke a sand grain was 13.6 N and the minimum was 0.135 N. Regressions of breaking force with length, width and thickness gave low r^2 values (0.18, 0.23 and 0.28, respectively). Multivariate regression with all three size variables did not explain more of the variation (r^2=0.29). Using thickness alone as the independent variable, breaking force=(0.02×thickness)+0.209. The slope is not zero (P=0.0003), indicating that larger sand grains require larger forces to break them. It should be noted that this is not a 'strength of material' test: it is merely an estimate of the forces required to break sediment particles.

Experiments with other clypeasteroids

The only other live specimens from which we were able to collect data were three *Encope michelini*. All devoured assorted urchin spines and *Halimeda* fragments in the laboratory. Two of them fractured the small microcells (6.7 N) and the third also broke the larger ones (13.6 N).

Lantern measurements were obtained from three other species (Table 3) and used to estimate probable forces along their teeth, assuming the muscle stress already determined for *C. rosaceus*.

Table 3. *Maximum biting forces predicted in different clypeasteroids, assuming the wedge model and using maximum muscle stress inferred for* Clypeaster rosaceus *(see text)*

Species	Body diameter (mm)	Predicted force (N)	Other data
Encope michelini	109.5	15.7	13.6 N (glass)
Mellita quinquiesperforata	77.0	7.3	6.2 N (sand)
Leodia sexiesperforata	86.6	7.1	3.9 N (*Halimeda*)
Echinarachnius parma	75.5	4.4	No data

The known performance capability of each species is listed in the final column (other data).

Discussion

Models of force generation by the lantern

In the following discussion we develop equations relating the force exerted by the teeth on the food with the stress exerted by the comminator muscles on the pyramids. Here, our objectives are: (1) to explain how circumferentially (tangentially) directed muscles can provide radial forces exerted by the teeth; (2) to predict the stresses required in the comminator muscles to provide the forces measured at the teeth; and (3) to identify morphological features required by this force-generating mechanism.

The jaws function like a five-sided 'vice grip'. The motion by which the teeth grip the food and exert force comes from the action of the interpyramidal (comminator) muscles (Fig. 1). Contraction of the comminator muscles causes the pyramids to slide or swing radially inwards until the teeth contact the food. Once the food is contacted, stress developed by the comminator muscles is directed radially by the pyramids to the teeth. When enough force is developed, the food is crushed.

Morphological correspondence between lantern and models

The geometry of the models is an abstraction of the morphology of the lantern. The correspondence between real lantern features and the simplified geometry of the models is shown in Figs 1–4. The lantern consists of five pyramids (Fig. 1) supporting teeth which protrude radially inwards (Figs 1 and 2). The teeth abut the pyramids in a tilted, curved plane (Fig. 3). Where the comminator muscles are attached (Fig. 2), each pyramid is expanded vertically relative to the suture area between the two half-pyramids. Thin ridges of calcite stretch from this expanded section to the sutural region (Fig. 1), terminating more or less centrally. Finally,

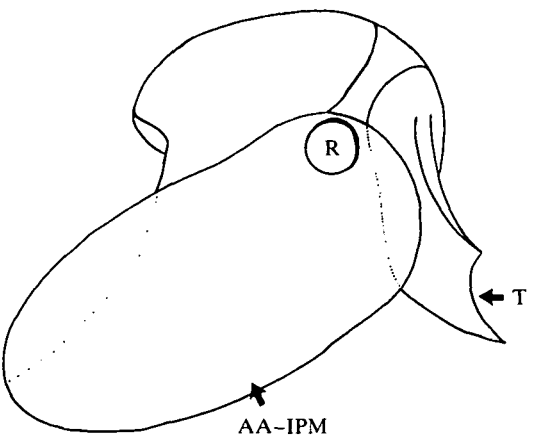

Fig. 3. Abstraction of a pyramid with tooth. The tip of the tooth (T) is supported by the pyramid along a horizontally curved but vertically straight surface which defines the location of r_i. The geometry of the real lantern is reduced by steps to the simplified geometry of the models. Both wedge and thick-walled cylinder models ignore the possible role of the rotule (R). AA–IPM, area for attachment of interpyramidal muscles.

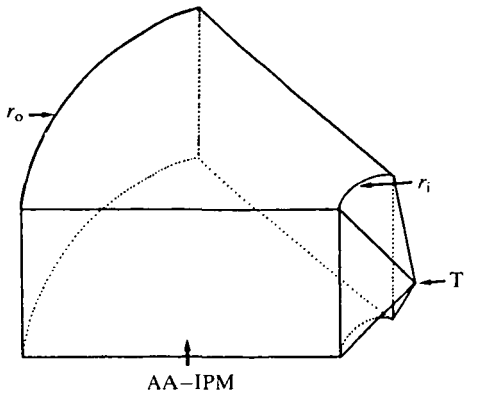

Fig. 4. Further abstraction of the pyramid as a pie-shaped section of a cylinder wall with a prism-shaped tooth (T). The length of the pie-shaped piece is $r_o - r_i$, and its angular width is given by 2α, where α is half the angle swept out by the pyramid. AA–IPM, area for attachment of interpyramidal muscles.

the distal edge of the pyramid extends further where the comminator muscles are located than where the half-pyramids meet.

Ignoring much of this detail, the models assume that the pyramid is a wedge cut from the wall of a thick-walled cylinder. The outer and inner margins of the pyramid are treated as arcs and the tooth as a prism (Fig. 4). In the real lantern, the outer margin forms part of a five-sided star. In addition, the inner margin departs from the cylindrical model in two ways: (i) it is more like the sloping wall of a cone, and (ii) the comminator muscles extend slightly towards the centre.

Force balance on the tooth

In both models, stress exerted over the contact area between the pyramid and the tooth is balanced by force exerted by food particles on the tooth (Fig. 5). This balance is given by:

$$F = 2\sigma_r l r_i \sin\alpha\,, \tag{1}$$

where F is the force exerted by a food particle on the tooth, σ_r is the radial stress at the plane where stress is transferred from the pyramid to the tooth, l is the height of the pyramid, r_i is the inside radius of the cylinder, and α is half the angle swept out by the pyramid.

Relationship between radial and tangential stresses

The radial stress that a pyramid exerts on a tooth, σ_r, is developed by tangential stress in the comminator muscle. If stresses are transmitted radially within the muscles, a thick-walled cylinder model is required. If radial stresses are not transferred in the comminator muscles, then a wedge model is required.

The thick-walled cylinder model

A thick-walled cylinder can be thought of as a series of thin-walled cylinders one

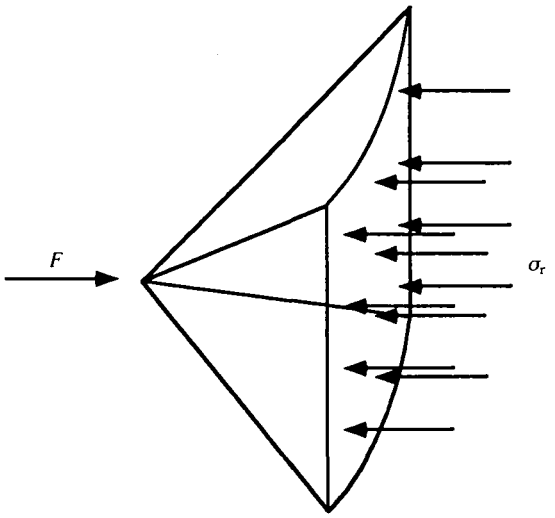

Fig. 5. Force balance on a tooth. Radial stress from the pyramid is balanced by force exerted on the tip of the tooth (see equation 1 in the text). F, the force exerted by a food particle on the tooth; σ_r, radial stress.

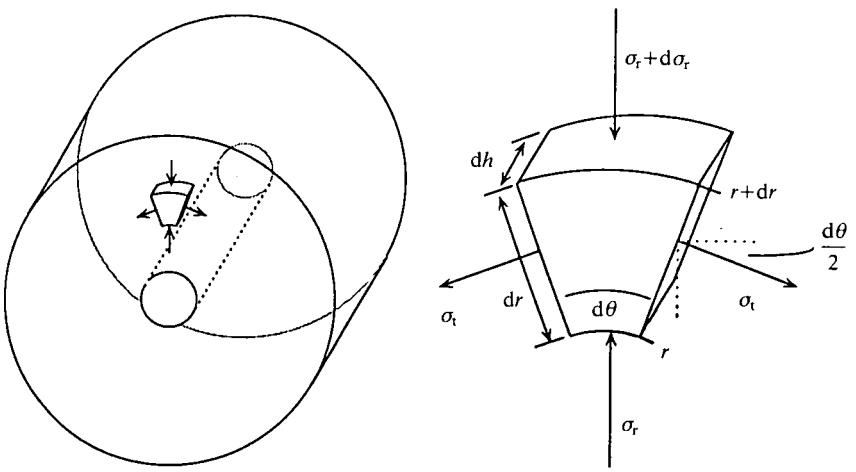

Fig. 6. Force balance for a thick-walled cylinder. An infinitesimal piece from inside the thick-walled cylinder has a balance between the forces from radial stresses on the inside and outside surfaces and a parallel component of forces from tangential stresses. The piece has dimensions dh, dr, $d\theta$. Force balance is:

$$\sigma_r h r d\theta - (\sigma_r + \frac{d\sigma_r}{dr} dr)(r+dr)h d\theta = -2\sigma_t h dr \frac{d\theta}{2}.$$

inside the other. The force balance for an infinitesimal element from one of these cylinders is shown in Fig. 6. A differential equation is required to find the radial (σ_r) and tangential (σ_t) stresses anywhere within the wall of the cylinder [see

derivations and assumptions in Popov (1976), Timoshenko and Goodier (1951), Higdon *et al.* (1978)]. These stresses are given by:

$$\sigma_t = p_i \frac{r_i^2}{r_o^2 - r_i^2}\left(1 + \frac{r_o^2}{r}\right), \tag{2}$$

and

$$\sigma_r = p_i \frac{r_i^2}{r_o^2 - r_i^2}\left(1 - \frac{r_o^2}{r}\right), \tag{3}$$

where p_i is the pressure inside the cylinder, r_o and r_i are the outside and inside radii, respectively, and r is the radial distance of the element from the centre of the cylinder.

In equations 2 and 3, σ_t is always larger than σ_r for a given value of r. Maximum tangential stress occurs at the inner edge of the cylinder and is:

$$\sigma_{t,max} = p_i \frac{r_o^2 + r_i^2}{r_o^2 - r_i^2}. \tag{4}$$

In the lantern, p_i is analogous to the radial stress, σ_r, exerted by the teeth on the pyramid. Using the analogy and substituting equation 1 into equation 4,

$$\sigma_{t,max} = \frac{F}{2lr_i \sin\alpha} \frac{r_o^2 + r_i^2}{r_o^2 - r_i^2}, \tag{5}$$

we can relate the comminator muscle stress to the dimensions of the lantern and the force produced at the teeth. Since $2lr_i\sin\alpha$ is the projected area of the surface where the tooth joins the pyramid, in practice we measured that area, the dimensions of the lantern and the force, and then used equation 5 to calculate the muscle stress.

We have assumed that the height of the comminator muscle is uniform with increasing radius. This is not generally so and our thick-walled cylinder will give an incorrect stress estimate as a result. Derivation of a model that allows for varying height of the comminator muscles is difficult. We have been able to find only one derivation applicable to a cylinder with such non-planar end faces (Nemish and Bloshko, 1986). This analysis shows that if the height decreases with increasing r, the stress distribution will be slightly flattened, producing relatively lower maximum stresses. This derivation is valid only for small variations in height. It is not possible to give a precise statement of how the predicted maximum stress would differ if the actual variation in height of the interpyramidal muscle was taken into account.

The lantern must be considered as a thick-walled rather than a thin-walled cylinder. A free-body diagram for a thin-walled cylinder is shown in Fig. 7. The relationship between radial and tangential stresses (Popov, 1976) is given by:

$$\sigma_r = \frac{\sigma_t \Delta t}{r}, \tag{6}$$

where σ_r is the radial stress, σ_t is the tangential stress, Δt is the wall thickness and r

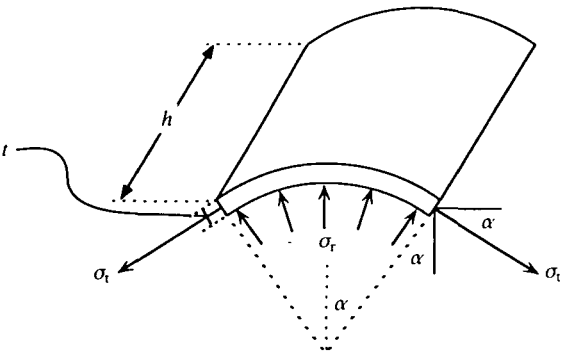

Fig. 7. Force balance for a section of thin-walled cylinder. Tangential stresses, σ_t, produce an inward radial component of force. These forces are balanced by outward radial stresses, σ_r, exerted on the inside of the cylinder. h is the height of the shell, t is the thickness, α is half the angle swept out by the shell. Force balance is:

$$2\sigma_t ht\sin\alpha = 2\sigma_r hr\sin\alpha .$$

is the radius (it does not matter whether one uses the outside or the inside radius). This formula is valid only as long as the wall thickness is small. The tangential stress predicted by equation 6 is considerably lower than the prediction for a thick-walled cylinder using equation 4. For a given ratio $r_o/r_i=k$, the ratio $\sigma_{thick}/\sigma_{thin}$ can be calculated. Using equations 5 and 6, for a thick-walled cylinder experiencing only an internal pressure, the maximum tangential stress is:

$$\sigma_{thick,max} = p_i \frac{r_o^2 + r_i^2}{r_o^2 - r_i^2} . \tag{7}$$

For a thin-walled cylinder experiencing only an internal pressure it is:

$$\sigma_{thin,max} = \sigma_t = r_i p_i / t . \tag{8}$$

Replacing r_o with kr_i:

$$\frac{\sigma_{thick,max}}{\sigma_{thin,max}} = (k^2+1)/(k+1) \tag{9}$$

The following is a table which gives this ratio for several examples:

$\frac{r_o}{r_i}=$	1	1.1	1.2	1.4	1.6	1.8	2.0	2.5	10
$\frac{\sigma_{thick,max}}{\sigma_{thin,max}}=$	1	1.05	1.10	1.23	1.37	1.51	1.67	2.07	9.18

For clypeasteroid lanterns r_o/r_i ranges between 3 and 10, depending on the species. Hence, the error from use of a thin-walled model becomes unacceptably large.

However, the stress distribution in the thick-walled cylinder model includes several assumptions that may not be met. We assume that the stress in the wall of

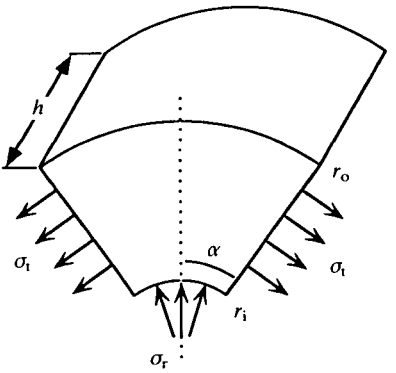

Fig. 8. Force balance for a wedge. The vertical component of forces from radial stresses exerted by the tooth on the pyramid is balanced by the vertical component of forces from tangential stresses exerted by the comminator muscles on the pyramid. Force balance is:

$$2\sigma_r l r_i \sin\alpha = 2\sigma_t l(r_o - r_i)\sin\alpha .$$

the cylinder is transferred the same way in the comminator muscle as in the pyramid. This may not be the case; for instance, it is possible that there are no radial forces transferred within the comminator muscles. The distribution of forces might then be quite different, and for this reason we derive another model.

The wedge model

This model assumes that the comminator muscles pull at right angles to the surface of the pyramid (Fig. 8). There are no shearing or radial forces allowed where the muscle attaches to the pyramid. Tangential stresses generated in the comminator muscles are balanced by stresses on the plane joining the pyramid to the tooth. The force delivered by the tooth is given by:

$$F = 2\sigma_t l(r_o - r_i)\sin\alpha . \tag{10}$$

The area of the comminator muscles involved is assumed to be rectangular and equal to $l(r_o - r_i)$. In fact, it does not matter what shape this area is: the component of the force developed is the same regardless of its radial location. Therefore, we can use the cross-sectional area of the muscle, the measured force and equation 10 to calculate stress in the comminator muscles.

Morphological predictions of the cylinder model

Substituting $f = r_o/r_i$ in equation 1:

$$F = 2\sigma_r l \frac{r_o}{f}\sin\alpha , \tag{11}$$

and, in equation 4 for the maximum tangential stress in a thick-walled cylinder, we obtain:

$$\sigma_t = \sigma_r \frac{f^2+1}{f^2-1}, \tag{12}$$

and

$$\sigma_r = \sigma_t \frac{f^2-1}{f^2+1}. \tag{13}$$

Then, using equation 13 in equation 11, we get:

$$F = \sigma_t \frac{f^2-1}{f^2+1} 2l \frac{r_o}{f} \sin\alpha. \tag{14}$$

Thus, the scaled ratio of tangential stress to force is:

$$\mathscr{F} = \frac{\sigma_t 2lr_o \sin\alpha}{F} = \frac{(f^2+1)f}{f^2-1}. \tag{15}$$

Equation 15 has one minimum in the region of interest. By taking the derivative with respect to f of function 15 and finding the zero values, we can find the minimum tangential stress required to produce a given radial force. This minimum, calculated by iteration, occurs at f=2.058, at which point the ratio, $\mathscr{F}$, is 3.330. To get the maximum force from a given muscle stress the jaw should have an external radius that is twice the internal radius.

The minimum in $\mathscr{F}$ is a result of the trade-off between the size of the tooth and the size of the pyramid. For a given external radius of jaw, there is an internal radius that will maximize the tooth size without making the lantern a thin-walled cylinder. When a thick-walled cylinder becomes thinner walled (r_i approaches r_o), the ratio of maximal tangential stress (equation 7) to the internal pressure (or the radial stress exerted on the cylinder by the teeth) increases steeply.

Morphological predictions of the wedge model

Substituting $f=r_o/r_i$ in equation 10 we get:

$$F=2\sigma_t l\left(r_o-\frac{r_o}{f}\right)\sin\alpha = 2\sigma_t l r_o\left(1-\frac{1}{f}\right)\sin\alpha, \tag{16}$$

and the ratio of tangential stress, σ_t, to the force produced at the tip of the tooth is:

$$\frac{\sigma_t}{F} = \frac{1}{2lr_o\,(1-\frac{1}{f})\sin\alpha}. \tag{17}$$

If we scale this ratio to account for the overall size of the jaw (wedge plus tooth) and the angle of the wedge (dependent on the number of teeth), we arrive at a comparable dimensionless number:

$$\mathscr{F} = \frac{\sigma_t 2lr_o \sin\alpha}{F} = \frac{1}{(1-\frac{1}{f})} = \frac{f}{f-1}. \tag{18}$$

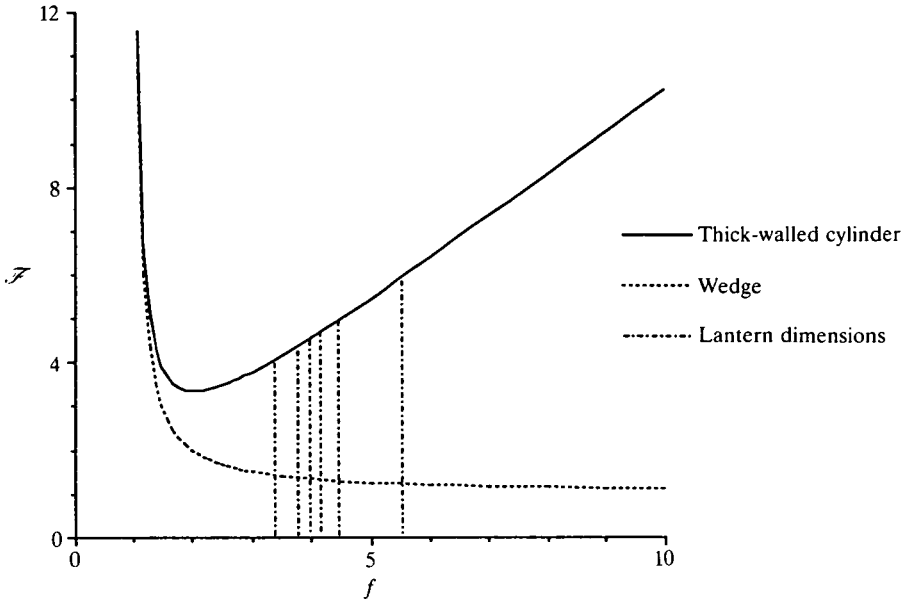

Fig. 9. $\mathscr{F}$, the ratio of the muscle stress to the force produced, appropriately scaled for the angular size of the pyramids (72°) and the size of the lantern, plotted against the ratio of the external to internal radii, f. Theoretical curves for wedge (dashed) and thick-walled cylinder (solid) model. Vertical lines show actual ratios from individuals of *Clypeaster rosaceus* in this study. This graph shows that a given force can be produced at the tip of the tooth by a smaller muscle stress if the wedge model is correct and the animal is thick-walled, or if the cylinder model is correct and the animal has an f of about 2.

This relationship is shown in Fig. 9. The size-specific force generated by a given muscle stress is thus dependent upon the proportions of the jaw, specifically the ratio of the outside to the inside diameter (f). This function takes into account both the effect of changing the length of the tooth and of changing the proportions of the jaw. As f increases from 1 to 2, there is a very rapid decline in the muscle stress required to produce a given force. Thus, if the goal is to produce a large force relative to the stress available, the lantern should have $f>2$. For very large values of f there is not much decrease in $\mathscr{F}$ with an additional increase in f. Fig. 9 shows $\mathscr{F}$ as a function of f and indicates the position along the f-axis of the specimens of *C. rosaceus* used in this study. The f-axis represents a one-dimensional morphospace. The models make predictions of where in that morphospace the animals should be found if the design maximizes the force produced at the tooth tip for a given comminator muscle stress.

The wedge model is more likely to be correct than the thick-walled cylinder because the ratio f (r_o/r_i) is generally higher in the animals than the optimum predicted for a thick-walled cylinder ($f=2.058$) and, in addition, the required muscle stress is lower in the wedge model. There are many assumptions in both models and some ambiguity in the location of r_o and r_i, which affects the

determination of f. Since the animals may not have the optimal design according to the criteria we chose, caution should be exercised in concluding that the wedge model is definitely better. Whichever model we choose, it is quite clear that there are tremendous disadvantages to being thin-walled. To make up for being thin-walled, a lantern would have to be very much taller, as is indicated by the rapid increase in $\mathscr{F}$ as f approaches 1 (Fig. 9).

Implications of models for forces and muscle stresses

The two models differ in predicted comminator muscle stress. The ratio of the muscle stress predicted in the thick-walled cylinder and in the wedge models is:

$$\frac{\sigma_{t,twc}}{\sigma_{t,wedge}} = \frac{f(f^2+1)}{(f^2-1)} \frac{f}{(f-1)}. \tag{19}$$

For f=3, this ratio is 5.625; as f approaches infinity, the ratio tends towards f. Therefore the thick-walled cylinder model predicts higher stresses in the comminator muscles than does the wedge model. In the range of f values concerned, the difference is not large enough to allow us to choose between the models at present. A more direct measurement of the capabilities of the comminator muscle might allow us to distinguish more clearly between these two models.

Maximum muscle stress calculated for the thick-walled cylinder model (equation 5), using the maximum force generated by *C. rosaceus*, was $2.8\times10^6\,N\,m^{-2}$, based on glass-fracturing tests. The maximum muscle stress for the wedge model (equation 10) was $1.9\times10^5\,N\,m^{-2}$. Thus, muscle stresses in the wedge model are very similar to the maximum reported values for vertebrates (1.6×10^5 to $2.9\times10^5\,N\,m^{-2}$) (McMahon, 1984), whilst the cylinder model yields values close to those cited for molluscan muscle (1.0×10^6 to $1.4\times10^6\,N\,m^{-2}$) (Schmidt-Nielsen, 1983).

Comparison of forces in Encope michelini *with those predicted by the models*

Applying the maximum stresses estimated above for *C. rosaceus* comminator muscles, we can predict the expected radial forces in the lanterns of other clypeasteroids (Table 3). For *Encope michelini*, using the wedge model, the predicted radial force along the teeth is 15.7 N. Their observed ability to fracture glass microcells (requiring 13.6 N) is thus within the expected range. Predicted lantern forces and known capabilities of other sand dollars are also shown in Table 3.

Ecological considerations

The role of the lantern in clypeasteroids has not been well understood. Goodbody (1960), Lane (1977) and Smith (1984) doubted that it was involved in feeding. Our own earlier work (Telford *et al.* 1985) provided evidence that the lantern fractures much of the ingested food material. The force measurements in this paper now show that there is no special 'trick' involved, such as selection of weak particles or prescoring them. Clypeasteroids simply exert sufficient brute

force to crush sand grains. Siliceous grains may already have inherent microfracture planes (Leeder, 1982) and carbonate grains are frequently penetrated by filaments of algae or bored by sponges, which greatly weakens them. Our results suggest that larger particles require larger forces than do small ones to fracture them. The size range of particles ingested by clypeasteroids depends largely on the size of the food-collecting podia (Telford and Mooi, 1986; Telford *et al.* 1987). Thus, both collection and fracture of grains are size-dependent. Clypeasteroids often occur in sufficient density for their grain-fracturing activity to be significant in resource recycling and the redistribution of grain sizes available to other deposit feeders.

Generality of models

Many features of the lantern which may be mechanically significant have been ignored by our models. For instance, there are thin calcite ridges leading from the comminator muscle planes to the centers of the pyramids. These appear to be stress-concentration ridges which might increase the effectiveness of the comminator muscle at each radius. Moments have also been ignored in our analysis. The placement of the retractor and protractor muscles, and the vertical placement of the pyramids seem likely to be affected by moments generated by forces on the teeth and by the comminator muscles. Furthermore, the rotules may act as pivots about which the pyramids could rotate as the teeth close on a particle. Such a rotation would imply that vertical placement of the comminator muscles was important in determining the total force exerted on the tooth. In fact, clypeasteroids may get considerable leverage from such an arrangement. These more complicated considerations have been deferred for future investigations: we note here only that they might have profound influence for muscle stresses and for morphological features in the models.

This work was supported by the Natural Sciences and Engineering Research Council of Canada through operating grant no. A 4696. We thank S. Vogel, Duke University, for the loan of his minicrusher, and J. Gosline, University of British Columbia, for use of his Instron maxicrusher. Lantern illustrations were drawn by R. Nakamura. We are grateful to the Marine Science and Conservation Center, Long Key, Florida, for letting us use their excellent facilities and boats. Finally we thank J. Covell, J. Gosline, A. S. Harold, A. Johnson, R. D. Mooi, A. Moore and C. Nichols for helpful discussions and critically reading the manuscript.

References

CANDIA CARNEVALI, M. D., LANZAVECCHIA, G., MELONE, G. AND CELENTANO, F. C. (1988). Aristotle's lantern in the regular sea urchin *Paracentrotus lividus*. II. Biomechanical approach to the interpretation of movement. *Proc. Int. Echinoderms Conf.*, Victoria, British Columbia, 1987. pp. 663–672. Rotterdam: A. A. Balkema.

ELLERS, O. AND TELFORD, M. (1984). Collection of food by oral surface podia in the sand dollar, *Echinarachnius parma* (Lamarck). *Biol. Bull. mar. biol. Lab., Woods Hole* **166**, 574–582.

GOODBODY, I. (1960). The feeding mechanism in the sand dollar, *Mellita sexiesperforata* (Leske). *Biol. Bull. mar. biol. Lab., Woods Hole* **119**, 80–86.

HIGDON, A., OHLSEN, E. H., STILES, W. B., WEESE, J. A. AND RILEY, W. F. (1978). *Mechanics of Materials*. 3rd edn. New York: John Wiley & Sons. 752pp.

HYMAN, L. H. (1955). *The Invertebrates*. IV. *Echinodermata*. New York: McGraw Hill. 763pp.

JENSEN, M. (1985). Functional morphology of test, lantern, and tube feet ampullae system in flexible and rigid sea urchins (Echinoidea). *Proc. Int. Echinoderms Conf.,* Galway, Eire, 1984. pp. 281–288. Rotterdam: A. A. Balkema.

KIER, P. (1974). Evolutionary trends and their functional significance in the post-Paleozoic echinoids. *J. Paleontol.* **48**(Suppl.). *Paleontol. Soc. Mem.* **5**, 1–95.

LANE, J. M. (1977). Bioenergetics of the sand dollar, *Mellita quinquiesperforata* (Leske, 1778). PhD dissertation, Department of Biology, University of South Florida, Tampa.

LANZAVECCHIA, G., CANDIA CARNEVALI, M. D., MELONE, G. CELANTANO, F. C. (1988). Aristotle's lantern in the regular sea urchin. *Paracentrotus lividus*. I. Functional morphology and significance of bones, muscles and ligaments. *Proc. Int. Echinoderms Conf.,* Victoria, British Columbia, 1987. pp. 649–662. Rotterdam: A. A. Balkema.

LAWRENCE, J. M. (1987). *A Functional Biology of Echinoderms*. Baltimore: Johns Hopkins University Press. 340pp.

LEEDER, M. R. (1982). *Sedimentology: Process and Product*. London, Allen & Unwin. 344pp.

MÄRKEL, K. (1970). Morphology of sea urchin teeth. IV. The teeth of *Laganum* and *Clypeaster* (Echinodermata: Echinoidea). *Z. Morph. Tiere* **88**, 370–389.

MCMAHON, T. A. (1984). *Muscle, Reflexes and Locomotion*. Princeton: Princeton University Press. 331pp.

MOOI, R. J. (1987). A cladistic analysis of the sand dollars (Clypeasteroida: Scutellina) and the interpretation of heterochronic phenomena, PhD dissertation, Department of Zoology, University of Toronto, Toronto, Canada. 208pp.

NEMISH, Y. N. AND BLOSHKO, N. M. (1986). Stressed state of elastic hollow cylinders with nonplanar end-faces. Institute of Mechanics, Academy of Sciences of the Ukranian SSR, Kiev (also called *Soviet Applied Mechanics*, 108–114), translated from *Prikladnaya Mekhanika*, **22**, 17–23.

POPOV, E. P. (1976). *Mechanics of Materials*, 2nd edn. Englewood Cliffs: Prentice-Hall. 590pp.

SCHMIDT-NIELSEN, K. (1983). *Animal Physiology: Adaptation and Environment*. 3rd edn. Cambridge: Cambridge University Press. 619pp.

SMITH, A. B. (1984). *Echinoid Palaeobiology*. London: George Allen & Unwin. 190pp.

SOKAL, R. R. AND ROHLF, F. J. (1981). *Biometry*. 2nd edn. San Francisco: W. H. Freeman. 859pp.

TELFORD, M., HAROLD, A. S. AND MOOI, R. (1983). Feeding structures, behaviour and microhabitat of *Echinocyamus pusillus* (Echinoidea: Clypeasteroida). *Biol. Bull. mar. biol. Lab., Woods Hole* **165**, 745–757.

TELFORD, M. AND MOOI, R. (1986). Resource partitioning by sand dollars in carbonate and siliceous sediments: evidence from podial and particle dimensions. *Biol. Bull. mar. biol. Lab., Woods Hole* **171**, 197–207.

TELFORD, M., MOOI, R. AND ELLERS, O. (1985). A new model of podial deposit feeding in the sand dollar, *Mellita quinquiesperforata* (Leske): the sieve hypothesis challenged. *Biol. Bull. mar. biol. Lab., Woods Hole* **169**, 431–448.

TELFORD, M., MOOI, R. AND HAROLD, A. S. (1987). Feeding activities of two species of *Clypeaster* (Echinoides: Clypeasteroida): further evidence of clypeasteroid resource partitioning. *Biol. Bull. mar. biol. Lab., Woods Hole* **172**, 324–336.

TIMOSHENKO, S. AND GOODIER, J. N. (1951). *Theory of Elasticity*. 2nd edn. New York: McGraw-Hill. 506pp.